

# Journal of Materials Chemistry A

Accepted Manuscript



This is an *Accepted Manuscript*, which has been through the Royal Society of Chemistry peer review process and has been accepted for publication.

*Accepted Manuscripts* are published online shortly after acceptance, before technical editing, formatting and proof reading. Using this free service, authors can make their results available to the community, in citable form, before we publish the edited article. We will replace this *Accepted Manuscript* with the edited and formatted *Advance Article* as soon as it is available.

You can find more information about *Accepted Manuscripts* in the [Information for Authors](#).

Please note that technical editing may introduce minor changes to the text and/or graphics, which may alter content. The journal's standard [Terms & Conditions](#) and the [Ethical guidelines](#) still apply. In no event shall the Royal Society of Chemistry be held responsible for any errors or omissions in this *Accepted Manuscript* or any consequences arising from the use of any information it contains.

# Solid–state dye–sensitized solar cells from poly(ethylene oxide)/polyaniline electrolytes with catalytic and hole–transporting characteristics

Yanyan Duan,<sup>a,b</sup> Qunwei Tang,<sup>a,b\*</sup> Yuran Chen<sup>b</sup>, Zhiyuan Zhao<sup>b</sup>, Yang Lv<sup>b</sup>, Mengjin Hou<sup>b</sup>, Peizhi Yang<sup>d</sup>, Benlin He<sup>b\*</sup>, Liangmin Yu<sup>a,c\*</sup>

<sup>a</sup> Key Laboratory of Marine Chemistry Theory and Technology, Ministry of Education, Ocean University of China, Qingdao 266100, P.R. China;

<sup>b</sup> Institute of Materials Science and Engineering, Ocean University of China, Qingdao 266100, P.R. China;

<sup>c</sup> Qingdao Collaborative Innovation Center of Marine Science and Technology, Ocean University of China, Qingdao 266100, P.R. China;

<sup>d</sup> Key Laboratory of Advanced Technique & Preparation for Renewable Energy Materials, Ministry of Education, Yunnan Normal University, Kunming 650092, P.R. China;

Tel/Fax: 86 532 66781690; Email address: tangqunwei@ouc.edu.cn; blhe@ouc.edu.cn;

yuyan@ouc.edu.cn

**Abstract:** Pursuit of cost–effective and efficient solid–state electrolytes is a persistent objective for dye–sensitized solar cells (DSSCs). We launch here the experimental design of iodide/triiodide ( $\Gamma/I_3^-$ ) incorporated poly(ethylene oxide)/polyaniline (PEO/PANi) solid–state electrolytes, aiming at expanding the catalytic event of  $I_3^-$  reduction from electrolyte/counter electrode interface to both interface and electrolyte system and shortening the charge diffusion path length. Except for  $\Gamma^-$  species, the conjugated PANi is also responsible for the dye regeneration and hole transfer to the

counte electrode. The DSSC with  $\Gamma/I_3^-$  incorporated PEO/1.0 wt% PANi electrolyte yields a maximum efficiency of 6.1% in comparison with 0.8% from PANi-free electrolyte-based solar cell and 0.1% for PANi-based solar cell.

## 1. Introduction

Solar energy, accounting for 99% of the total energy on the earth, has been considered as one of the promising green energy resources for developing low-carbon economy. The direct conversion of solar energy into electricity is an efficient solution to nowadays energy problems. Among diversified photovoltaic devices,<sup>1-4</sup> dye-sensitized solar cells (DSSCs) have received widespread attention as inexpensive and remarkably efficient energy conversion devices.<sup>5-8</sup> A typical DSSC configures an electrolyte containing redox couples dissolved in an organic solvent, which is sandwiched between an organic dye-sensitized  $TiO_2$  anode and a counter electrode (CE).<sup>9</sup> The nowadays highlights are focusing on understanding and improving charge generation, transport, recombination, and collection along with optimizing materials for liquid-electrolyte DSSC operation.<sup>10-12</sup> Till now, a maximum efficiency of 13% has been measured under air mass 1.5 (AM1.5) global sunlight.<sup>13</sup> Owing to the flaws in solvent leakage and evaporation, the mass production and long-term stability of such DSSC devices have been limited. One solution to this impasse is to employ microstructured polymer gel electrolytes with three-dimensional (3D) frameworks and all-solid-state electrolytes.<sup>14-17</sup> Although liquid electrolyte can be imbibed and remained in the 3D structures of polymer gel electrolytes by osmotic pressure or capillary force,<sup>18</sup> the dilemma of organic solvent evaporation is still unchanged. Therefore, the challenge of achieving commercial success will be in designing efficient all-solid-state electrolytes with facile synthesis processes and cost-effectiveness. The focus of the current solid-state systems is always on

enhancement of charge-transfer ability. An emerging avenue by our group is to explore conducting polymers or carbonaceous materials integrated electrolytes having catalytic activities for triiodide ( $I_3^-$ ) reduction. In our previous works,<sup>19,20</sup> conducting species such as polyaniline (PANi), polypyrrole, and graphene have been successfully imbedded into 3D frameworks of polymer gel electrolytes, aiming at extending reduction reaction of  $I_3^-$  from electrolyte/CE interface to whole structure thanks to a catalytic nature of such conducting polymers. Moreover, organic hole transporting materials (HTMs) such as 2,2',7,7'-tetrakis(*N,N*-di-4-methoxyphenylamino)-9,9'-spirobifluorene (*spiro*-OMeTAD) have also been employed to replace electrolytes,<sup>21,22</sup> which leads to > 5% efficiency for solid DSSCs. The oxidized dye can be regenerated by the hole injection into the HTM, which is subsequently collected by CE to fulfill an electronic circuit. These results demonstrate the great potential of developing solid-state DSSCs based on organic HTMs. Although *spiro*-OMeTAD is the most favorable organic HTM for such solid solar cells, it has suffered some defects in low hole mobility and high fabrication cost.<sup>23,24</sup> Consequently, conjugated polymers such as polyaniline have been investigated as the alternative HTM due to their thermal stability, high conductivity, good solubility as well as tunable optoelectronic features.<sup>25,26</sup>

To explore versatile full-solid-state electrolytes having catalytic and hole-transporting features, here we launch an experimental strategy of synthesizing simple composite electrolytes from  $I^-/I_3^-$  incorporated poly(ethylene oxide)/polyaniline (PEO/PANi) for solid-state DSSC application. The resultant PEO/PANi displays intrinsic electrocatalytic activity toward the reduction of  $I_3^-$  ions, rapid charge-transfer ability, easy synthesis, and cost-effectiveness, which demonstrates the merits of extraordinary solid-state electrolytes in efficient DSSCs. In addition, the integration of conjugated structure from PANi can shorten the charge diffusion path length. More importantly, the

conjugated PANi structures participate in the dye regeneration by hole injection into the PANi. To our knowledge, there are no systematic ageing studies on efficient DSSCs from solid-state electrolytes with catalytic and hole-transporting functions. The DSSC employing PEO/1.0 wt% PANi shows an efficiency as high as 6.1%, which is much higher than 0.8% from the cells with  $\Gamma/I_3^-$  incorporated PEO electrolyte and 0.1% for pristine PANi hole material.

## 2. Experimental

### 2.1 Synthesis of solid-state electrolytes

0.592 mL of aniline was dissolved in 20 mL of 1 M HCl aqueous solution to obtain a homogeneous mixture. 20 mL of 0.125 M ammonium peroxydisulfate aqueous solution was dipped in the above mixture within 30 min. The polymerization reaction was carried out at 0 °C. After 3 h, the resultant reactant was rinsed by 1M HCl aqueous solution, filtrated, and finally vacuum dried at 60 °C for 24 h. The feasibility of synthesizing  $\Gamma/I_3^-$  incorporated PEO/PANi electrolytes was confirmed by the following experimental procedures: A mixing solution consisting of  $\Gamma/I_3^-$  redox couples, PEO, and PANi was made by agitating 0.1 g of LiI, 0.019 g of  $I_2$ , 0.264 g of PEO ( $M_w = 2,000,000$ ), and stoichiometric PANi (The dosages of PANi were adjusted to be 0.2, 0.4, 0.6, 0.8, 1.0, and 2.0 wt% of PEO weight). After vigorous agitating for 24 h, the reactant with a viscosity of around 100 mPa s<sup>-1</sup> was casted onto dye-sensitized TiO<sub>2</sub> anode for consolidation at vacuum. As a reference, the  $\Gamma/I_3^-$  incorporated PEO electrolyte was also prepared according to the above approach at the same stoichiometric ratio.

### 2.2 Assembly of DSSCs

A layer of TiO<sub>2</sub> nanocrystal anode film with a thickness of ~10 μm was prepared by a sol-hydrothermal method.<sup>27</sup> The resultant anodes were further sensitized by immersing into a 0.50

mM ethanol solution of N719 dye. The DSSC was fabricated by sandwiching redox electrolyte between a dye-sensitized TiO<sub>2</sub> anode and a Pt CE (purchased from Dalian HepatChroma SolarTech Co., Ltd). A redox electrolyte consisted of 100 mM of tetraethylammonium iodide, 100 mM of tetramethylammonium iodide, 100 mM of tetrabutylammonium iodide, 100 mM of NaI, 100 mM of KI, 100 mM of LiI, 50 mM of I<sub>2</sub>, and 500 mM of 4-tert-butyl-pyridine in 50 ml acetonitrile. Surlyn film (30 μm) was utilized to seal the device through hot-pressing.

### 2.3 Electrochemical characterizations

The electrochemical performances were recorded on a conventional CHI660E setup comprising an Ag/AgCl reference electrode, a CE of Pt sheet, and a working electrode of FTO glass supported electrolyte. The CV curves were recorded in a supporting electrolyte consisting of 50 mM M LiI, 10 mM I<sub>2</sub>, and 500 mM LiClO<sub>4</sub> in acetonitrile. Bode phase measurements were carried out in a frequency range of 0.1 Hz ~ 10<sup>5</sup> kHz and an ac amplitude of 10 mV at room temperature. Both Bode plots and Tafel polarization curves were recorded by assembling symmetric dummy cell consisting of Pt CE|solid-state electrolyte|Pt CE.

### 2.4 Photovoltaic measurements

The photovoltaic test of the DSSC with an active area of 0.25 cm<sup>2</sup> was carried out by measuring the photocurrent-voltage (*J-V*) characteristic curves using a CHI660E Electrochemical Workstation under irradiation of a simulated solar light from a 100 W Xenon arc lamp (XQ-500 W) in ambient atmosphere. The incident light intensity was controlled at 100 mW cm<sup>-2</sup> (calibrated by a standard silicon solar cell). A black mask with an aperture area of around 0.25 cm<sup>2</sup> was applied on the surface of DSSCs to avoid stray light.

### 2.5 Other characterizations

The ionic conductivity of electrolyte was measured using a conductivity meter (DSSJ-308A, LeiCi Instruments) by consolidating electrolyte into interspace between two electrodes. The instrument was calibrated with 0.01 M KCl aqueous solution prior to experiments. Fourier transform infrared spectrometry spectra (FTIR) were recorded on a Vertex 70 FTIR spectrometer (Bruker).

### 3. Results and discussion

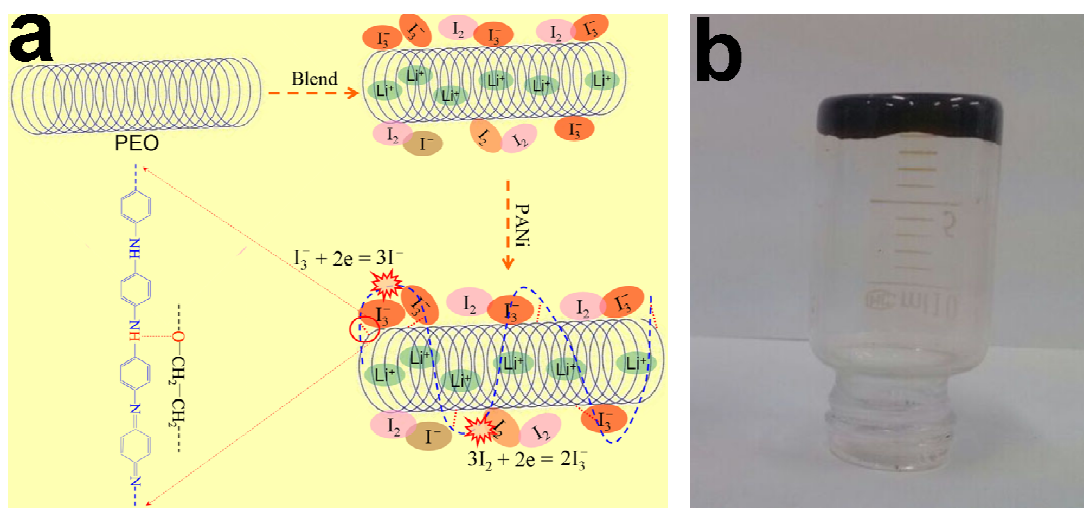


**Fig. 1** (a) Schematic illustration of synthesizing  $I^-/I_3^-$  incorporated PEO/PANi solid-state electrolytes. The PANi chains are bonded onto PEO backbones by H-bonding for catalyzing  $I_3^-$  reduction. (b) Digital photograph for inverted PEO/1.0 wt% PANi solid electrolyte.

Fig. 1a illustrates the synthesis process of  $I^-/I_3^-$  incorporated PEO/PANi solid electrolyte as well as H-bonding between PEO and PANi.<sup>28</sup>  $Li^+$  ions are embedded into free volume regions of PEO surrounded by  $I^-$  and  $I_3^-$  counter ions. The conformational transformation of PEO segments at relaxation motion precipitates the migration of  $Li^+$  and therefore  $I^-/I_3^-$  couples. Due to a redox nature of PANi, PANi nanostructures have been widely utilized as CE materials for Pt candidates.<sup>29–31</sup>

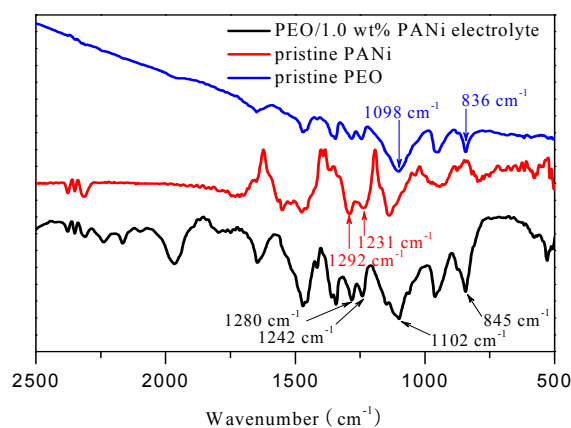


**Fig. 2** FTIR spectra of PEO/1.0 wt% PANi electrolyte, pristine PANi and PEO.

Spectroscopy techniques have been employed to examine the formation of functional bands and reaction mechanisms. The FTIR spectrum of the PEO/1.0 wt% PANi electrolyte is shown in Fig. 2. The observation of the bands at 800–900  $\text{cm}^{-1}$  indicates the occurrence of PANi polymerization via a head-to-tail mechanism.<sup>32</sup> The oxygenic species are expected to interact with the conjugated structure of PANi, especially through the Q-ring (semiquinone radical cation), as has been reported in the case of nanocrystalline  $\text{TiO}_2$  and Au.<sup>33</sup> Once the PANi is integrated with PEO, the bands belonging to C–N stretching the secondary aromatic amine, and C–N–C stretching vibration in the polaron structure move from 1292 and 1231  $\text{cm}^{-1}$  to 1280 and 1242  $\text{cm}^{-1}$ , respectively. Additionally, the bands for C–O–C stretching and C–O stretching at 1098 and 836  $\text{cm}^{-1}$  have also shifted to 1102 and 845  $\text{cm}^{-1}$ , respectively. These signal the interaction between PANi (C–N) and PEO (C–O–C) through H-bonds.

Close contact of PEO/PANi electrolyte with Pt electrode results in a conduction of reflux electrons (the electrons from external circuit to Pt CE) from Pt layer to the whole solid-state electrolyte. The conducting channels formed by PANi chains function as pathways for electron transfer and can be optimized by adjusting PANi dosage. Activated by electrons, PANi will catalyze the reduction reaction of  $\text{I}_3^-$  (Red<sub>1</sub>:  $\text{I}_3^- + 2e = 3\text{I}^-$ ) and  $\text{I}_2$  (Red<sub>2</sub>:  $3\text{I}_2 + 2e = 2\text{I}_3^-$ ), in which Red<sub>1</sub> governs the whole reaction kinetics. In order to demonstrate the solid nature of PEO/PANI, the

container having PEO/1.0 wt%PANi electrolyte is inverted, as shown in Fig. 1b, the electrolyte stays on the bottom of contain and no flow is observed, which is another solid support for solid-state PEO/PANi. Cyclic voltammetry (CV) is a commonly used technique in determining catalytic activity. The CV curve of the solid state electrolyte was measured by a conversional three-electrode system comprising a working electrode of Cu foil supported solid electrolyte, a CE of a Pt wire, and liquid electrolyte containing  $\Gamma^-/I_3^-$  redox couples. As shown in Fig. 3a, two pairs of redox peaks are observed in  $\Gamma^-/I_3^-$  incorporated PEO/1.0 wt%PANi solid-state electrolyte, the peak shape and positions are similar to pure PANi CE,<sup>29-31</sup> indicating that the solid-state PEO/PANi electrolyte has the same catalytic activity toward  $I_3^-$  reduction. As a reference, no redox peaks are detected from  $\Gamma^-/I_3^-$  incorporated PEO electrolyte, suggesting no catalysis of  $\Gamma^-/I_3^-$  incorporated PEO. With an aim of demonstrating the catalytic activity of solid electrolyte, the  $\Gamma^-/I_3^-$  incorporated PEO/PANi film is sandwiched between two Pt electrodes. As shown in Fig. 3b, the  $\tau$  of electrons at electrolyte/Pt electrode can be calculated by equation:<sup>34</sup>  $\tau = 1/2\pi f_p$ , where  $f_p$  is the second peak frequency. Once the electrons migrate from external circuit to Pt layer, they either participate in the  $I_3^-$  reduction at electrolyte/CE or transfer to PEO/PANi system, therefore, the average  $\tau$  of electrons can be utilized to compare the synthetical kinetics of Pt and PANi toward  $I_3^-$  reduction. Apparently, PEO/1.0 wt%PANi electrolyte exhibits a lifetime of 2.53 ms, as summarized in Table 1, which is shorter than that for other solid electrolytes.<sup>35,36</sup> Considering that Pt electrode has the same catalytic performance, the enhancement in synthetical kinetics reflects the highest catalytic activity in PEO/1.0 wt%PANi electrolyte. Fig. 3c shows Tafel polarization curves recorded on the same symmetrical dummy cell for Bode phase measurement. The slope for the anodic or cathodic branch represents exchange current density ( $J_0 = RT/nFR_{ct}$ ).<sup>37</sup> It is apparent PEO/1.0 wt%PANi electrolyte has a maximum  $J_0$  and therefore charge-transfer ability. Additionally, the intersection of cathodic

branch with  $Y$ -axis is a limiting diffusion current density ( $J_{lim} = 2nFCD_n/l$ ),<sup>38</sup> a parameter depending on the diffusion coefficient of  $I^-/I_3^-$  redox couples. The extracted  $J_{lim}$  and diffusion coefficient of redox species ( $D_n$ ) from PEO/1.0 wt% PANi are much higher than those of pure PEO electrolyte, indicating that the resultant ionic conductivity is significantly elevated.

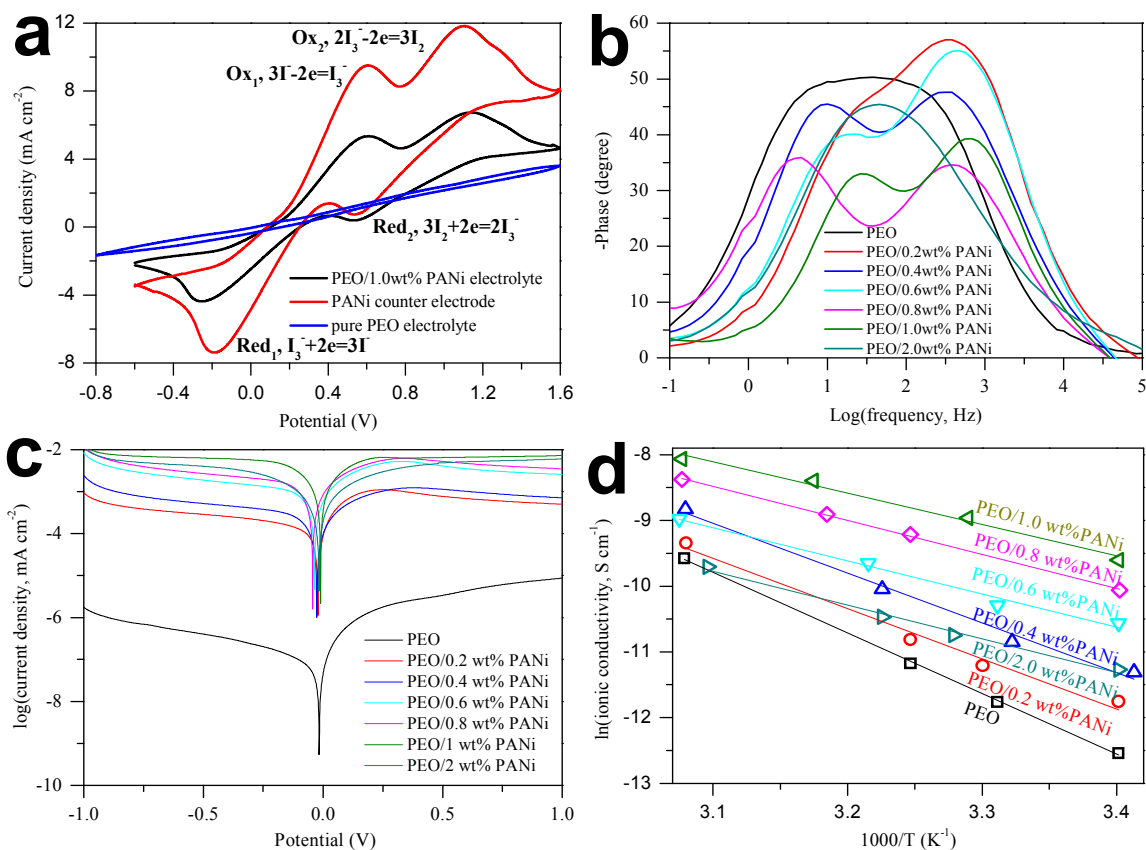


**Fig. 3** (a) CV curves of  $I^-/I_3^-$  incorporated PEO/1.0 wt% PANi solid-state electrolyte, PANi CE, and  $I^-/I_3^-$  incorporated PEO electrolyte, (b) bode phase plots and (c) Tafel polarization curves of symmetric dummy cells from solid electrolytes. (d) Temperature dependence of ionic conductivity for various solid-state electrolytes.

**Table 1** Parameters for electrochemical data and electron lifetime.

| Electrolytes     | $R_{ct1}$ ( $\Omega \text{ cm}^2$ ) | $R_{ct2}$ ( $\Omega \text{ cm}^2$ ) | $\tau$ (ms) | $W$ ( $\Omega \text{ cm}^2$ ) |
|------------------|-------------------------------------|-------------------------------------|-------------|-------------------------------|
| PEO              | 36.1                                | 621.9                               | —           | 255.2                         |
| PEO/0.2 wt% PANi | 21.6                                | 57.9                                | 4.59        | 123.0                         |
| PEO/0.4 wt% PANi | 9.13                                | 21.2                                | 4.55        | 108.7                         |
| PEO/0.6 wt% PANi | 9.08                                | 16.4                                | 3.93        | 31.9                          |
| PEO/0.8 wt% PANi | 8.82                                | 9.59                                | 3.90        | 20.4                          |

|                 |      |      |      |      |
|-----------------|------|------|------|------|
| PEO/1.0 wt%PANi | 4.19 | 5.72 | 2.53 | 7.74 |
| PEO/2.0 wt%PANi | 8.74 | 58.6 | 3.34 | 86.1 |

Another creative feature of PEO/PANi electrolyte is to shorten charge ( $I^-/I_3^-$  redox couples) diffusion path length. In the DSSC with pure PEO electrolyte, the  $I^-$  ions must migrate from electrolyte/Pt CE interface to electrolyte/anode interface for dye recovery, whereas the  $I_3^-$  species have to transfer across the whole electrolyte system to electrolyte/Pt CE for reduction. However, the event for cell device from PEO/PANi solid electrolyte becomes more energetic in accelerating  $I_3^- \leftrightarrow I^-$  conversion. Assisted by schematic diagram in Fig. 1, we can reveal the potential mechanism. It has been previously described that the interconnected channels from PANi chains distribute through the whole electrolyte, the  $I_3^-$  ions originated from electrolyte/anode interface only transfer to conjugated chain segments of PANi for reduction reaction instead of electrolyte/Pt CE interface. The as-reduced  $I^-$  species have also a short time of returning to electrolyte/anode interface. Therefore, we can make a conclusion that the integration of PANi can shorten the  $I^-/I_3^-$  diffusion path length. Although we can not determine the accurate path and length in the current study, it is still preliminarily pioneering to demonstrate new insights on how to elevate  $I_3^-$  reduction, shorten charge diffusion path length, and therefore markedly enhance photovoltaic performances of solid-state DSSCs.

The ionic conductivity of solid electrolyte is crucial to the photovoltaic performances of DSSC. Fig. 3(d) shows the temperature dependence of ionic conductivities for the solid-state electrolytes and the data are summarized in Table 2.  $I^-/I_3^-$  incorporated PEO/1.0 wt%PANi exhibits the highest conductivity of  $67.73 \mu\text{S cm}^{-1}$  at  $\sim 20^\circ\text{C}$  in comparison to  $3.59 \mu\text{S cm}^{-1}$  for  $I^-/I_3^-$  incorporated PEO. Compared with  $5.76 \text{ mS cm}^{-1}$  for ester-functionalized solid-state electrolyte,<sup>17</sup> the measured conductivity is still unimpressive, therefore the enhanced photovoltaic performances are responsible for the peculiar catalytic activity. The ionic conductivities of the electrolytes measured under dry air

from  $\sim 20$  to  $\sim 50$  °C follow an Arrhenius relationship:  $\sigma = \sigma_0 \exp(-E_a/RT)$ , where  $\sigma$  is ionic conductivity,  $E_a$  represents activation energy,  $T$  refers to absolute temperature,  $R$  is molar gas constant. It is found that all plots of  $\ln \sigma$  against  $1000/T$  give straight lines, which is a typical ion-conducting behavior. The  $E_a$ ,<sup>39</sup> which is the minimum energies required for ionic conduction through  $\Gamma^-/I_3^-$  incorporated PEO/PANi solid-state electrolytes at 0, 0.2, 0.4, 0.6, 0.8, 1.0, and 2.0 wt% PANi are obtained from the slopes in the linear fit, showing 76.66, 63.46, 63.07, 43.08, 41.98, 39.66, and 42.71 kJ mol<sup>-1</sup>, respectively. The  $E_a$  of the electrolyte at 1.0 wt% PANi is the lowest, indicating that ion ( $\Gamma^-$  and  $I_3^-$ ) movement becomes easier in  $\Gamma^-/I_3^-$  incorporated PEO/PANi system.

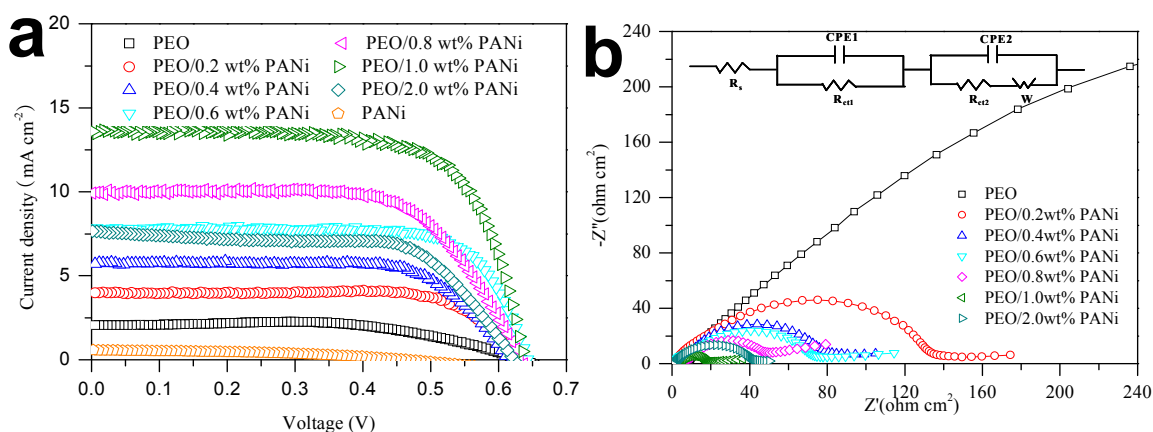


**Fig. 4** (a) Characteristic  $J-V$  curves and (b) Nyquist EIS plots of the DSSCs with solid electrolytes. The inset gives an equivalent circuit.  $R_s$ : sheet resistance;  $R_{ct1}$ : charge-transfer resistance at CE/electrolyte;  $R_{ct2}$ : charge-transfer resistance at  $\text{TiO}_2$ /electrolyte interface;  $W$ : Nernst diffusion resistance corresponding to the diffusion resistance of  $\Gamma^-/I_3^-$  redox couples; CPE1/CPE2: constant phase elements.

**Table 2** Photovoltaic parameters of DSSCs with varied solid-state electrolytes and the conductivity data.  $V_{oc}$ : open-circuit voltage;  $J_{sc}$ : short-circuit current density,  $FF$ : fill factor;  $\eta$ : power conversion efficiency;  $\sigma$ : ionic conductivity at  $\sim 20$  °C.

| Electrolytes     | $\eta$ (%) | $V_{oc}$ (V) | $FF$ (%) | $J_{sc}$ ( $\text{mA cm}^{-2}$ ) | $\sigma$ ( $\mu\text{S cm}^{-1}$ ) |
|------------------|------------|--------------|----------|----------------------------------|------------------------------------|
| PEO              | 0.8        | 0.633        | 61.4     | 2.06                             | 3.59                               |
| PEO/0.2 wt% PANi | 1.9        | 0.628        | 75.3     | 4.02                             | 7.87                               |

|                 |     |       |      |       |       |
|-----------------|-----|-------|------|-------|-------|
| PEO/0.4 wt%PANi | 2.5 | 0.616 | 71.2 | 5.70  | 12.26 |
| PEO/0.6 wt%PANi | 3.8 | 0.642 | 76.1 | 7.78  | 25.82 |
| PEO/0.8 wt%PANi | 4.2 | 0.633 | 66.9 | 9.92  | 42.84 |
| PEO/1.0 wt%PANi | 6.1 | 0.636 | 70.6 | 13.59 | 67.73 |
| PEO/2.0 wt%PANi | 3.1 | 0.623 | 65.1 | 7.64  | 12.76 |
| PANi            | 0.1 | 0.516 | 34.6 | 0.56  | 4.37  |

Fig. 4a displays  $J-V$  curves of the DSSCs using  $\Gamma^-/I_3^-$  incorporated PEO/PANi,  $\Gamma^-/I_3^-$  incorporated PEO solid electrolytes and pristine PANi hole-transporting material. The DSSC with PEO/1.0 wt%PANi electrolyte yields an optimal  $\eta$  of 6.1% ( $J_{sc} = 13.59 \text{ mA cm}^{-2}$ ,  $V_{oc} = 0.636 \text{ V}$ ,  $FF = 70.6\%$ ). The recorded efficiency is in a very high level for the solid-state DSSCs with either pristine solid-state electrolytes or HTMs.<sup>40-43</sup> It is noteworthy to mention that the efficiencies for the solar cells with  $\Gamma^-/I_3^-$  incorporated PEO and pristine PANi hole layer are 0.8% and 0.1%, respectively. The marked enhancement in efficiency is attributed to the synergistic effects of catalytic activity and shortened charge diffusion path length of PEO/PANi electrolyte and hole injection into PANi. Notably, the  $J_{sc}$ , having the same order to  $\eta$ , signals that the rapid interconversion between  $I_3^-$  and  $\Gamma^-$  can accelerate the generation of photoelectrons from dye molecules and therefore elevate the accumulative electron density on conduction band of  $\text{TiO}_2$ . The recorded efficiency from  $\Gamma^-/I_3^-$  incorporated PEO/1.0 wt%PANi is impressive in comparison with other full-solid-state DSSCs.<sup>27,35,44,45</sup> In comparison with liquid-system DSSCs, the efficiency is still modest. The dye regeneration by organic HTM is generally on the picosecond time scale and at least one order of magnitude faster than that in a typical liquid electrolyte device.<sup>46</sup> This means the charge separation and dye regeneration are not the major bottleneck for the low device performance of the resultant DSSCs. Other limitations such as low hole mobility of organic HTMs and incomplete filling of HTM into mesoporous  $\text{TiO}_2$  film have been considered because the derivative problems could lead to excessive interfacial recombination loss and dye regeneration hysteresis.

EIS experiments were carried out for the DSSCs to confirm the charge-transfer abilities of

resultant solid electrolytes. Nyquist plots in Fig. 4b illustrate that the  $R_{ct1}$  follows an order of PEO/1.0 wt% PANi ( $4.19 \Omega \text{ cm}^2$ ) < PEO/2.0 wt% PANi ( $8.74 \Omega \text{ cm}^2$ ) < PEO/0.8 wt% PANi ( $8.82 \Omega \text{ cm}^2$ ) < PEO/0.6 wt% PANi ( $9.08 \Omega \text{ cm}^2$ ) < PEO/0.4 wt% PANi ( $9.13 \Omega \text{ cm}^2$ ) < PEO/0.2 wt% PANi ( $21.6 \Omega \text{ cm}^2$ ) < PEO ( $36.1 \Omega \text{ cm}^2$ ), which is consistent with sequence of  $\tau$  and therefore catalytic activity. However,  $W$  represents the Nernst diffusion resistance of  $\Gamma^-/I_3^-$  redox couples. A lower  $W$  means that the  $\Gamma^-/I_3^-$  species have higher diffusion kinetics. The results of  $W$  match ionic conductivity well.

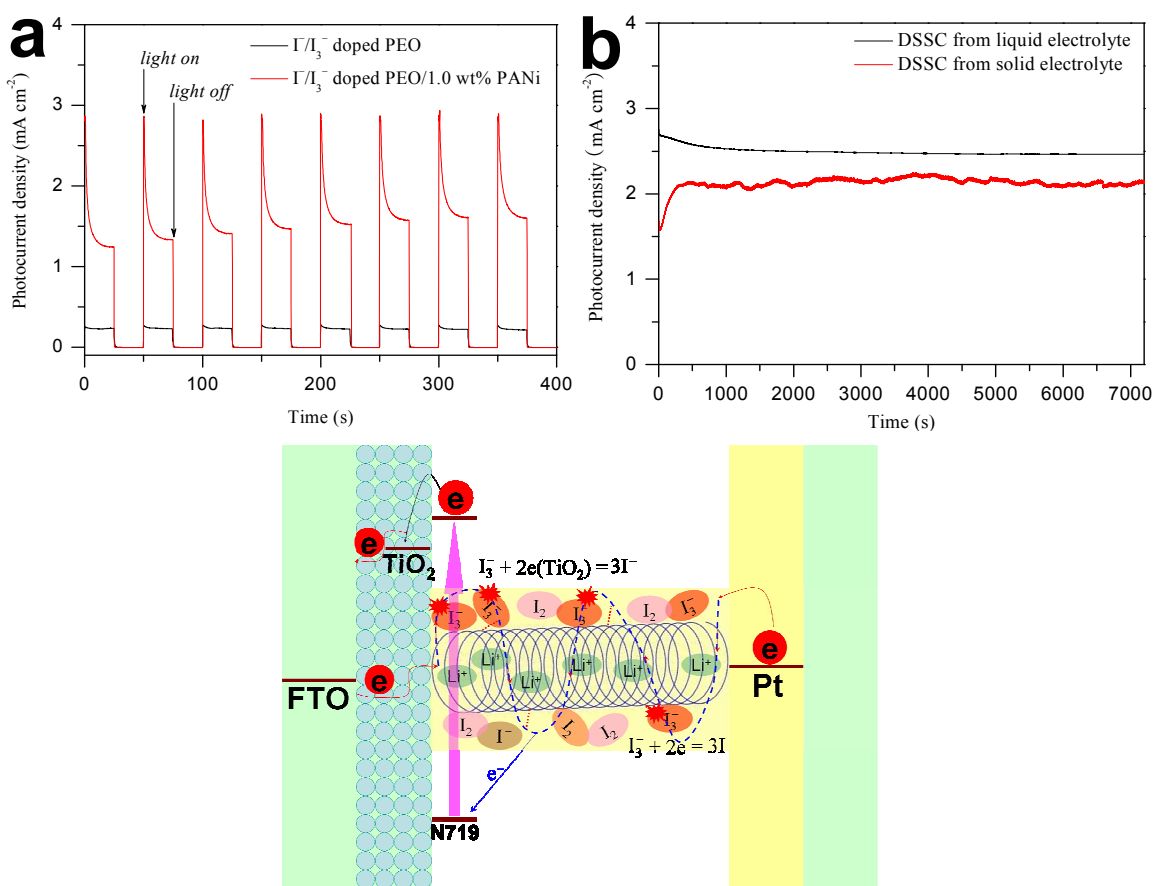


**Fig. 5** (a) The start–stop switches for the DSSCs with  $\Gamma^-/I_3^-$  incorporated PEO/1.0 wt% PANi and PEO solid electrolytes. (b) Photocurrent stabilities recorded on the DSSCs from traditional liquid electrolyte and  $\Gamma^-/I_3^-$  incorporated PEO/1.0 wt% PANi solid electrolyte. The schematic sketch illustrates the electron migration routes along PANi chains from Pt electrode and TiO<sub>2</sub> anode in a real solid–state DSSC.

When applied as windows, roof panels, or portable sources, the fast start-up, multiple start/stop cycles, and good photocurrent stability are prerequisite merits for solar panels. Fig. 5a exhibits the start-stop switches of cell device employing  $\Gamma^-/I_3^-$  incorporated PEO/1.0 wt% PANi electrolyte. As a reference, the switching of cell device with  $\Gamma^-/I_3^-$  incorporated PEO is also measured under the same conditions. An abrupt increase in photocurrent density at “light on” means the fast start-up of DSSC, whereas no delay in reaching the highest current density suggests that the incorporation of PANi with PEO accelerates hole injection and the interconversion between  $I_3^-$  and  $\Gamma^-$  as well as shortens the charge transfer path length. Interestingly, there is a depressed process in each “on” stage, indicating a diffusion-limited transport mechanism in the solid electrolytes. The schematic sketch in Fig. 5 illuminates the transfer avenues of electrons within a real solid-state DSSC employing  $\Gamma^-/I_3^-$  incorporated PEO/PANi electrolyte. Generally, the photogenerated electrons released from excited dye molecules have two feasibilities: (i) The majority of electrons flow to conduction band of  $TiO_2$  and further migrate to FTO layer along conducting channels; (ii) Only a minority of electrons transfer to  $TiO_2$ /electrolyte interface and suffer from recombination with  $I_3^-$  ions.<sup>47</sup> Due to a fact that PANi has an ability of conducting electrons, the electrons at  $TiO_2$ /electrolyte interface are expected to transfer to electrolyte layer along PANi chains and recombine with encountered  $I_3^-$ , resulting in a decreased electron density in  $TiO_2$  and therefore photocurrent density of a cell device. However, the conducted electrons from electrolyte/Pt interfaces participate in the reduction reaction of  $I_3^- + 2e \rightarrow 3I^-$ , accelerating the interconversion kinetics of  $I_3^-$  species. Although there is also a decreased process for the cell with  $\Gamma^-/I_3^-$  incorporated PEO electrolyte, the reduction degree is apparently confined in the absence of PANi, whereas the lower photocurrent density reflects a relatively poor  $\Gamma^-/I_3^-$  interconversion and therefore dye recovery kinetics. These conclusions are in an agreement with electrochemical and photovoltaic

characterizations. Moreover, the conjugated PANi can also participate in the dye regeneration by the hole injection into the PANi, which is also favorable to the photovoltaic performances. After eight start/up cycles, no obvious decrease in photocurrent density is observed, suggesting the solid-state DSSC has multiple start/up capability. In order to compare the stability of DSSCs with traditional liquid electrolyte containing  $\Gamma/I_3^-$  redox couples and  $\Gamma/I_3^-$  incorporated PEO/PANi electrolyte, their photocurrent stabilities are carried out by a chronoamperometry mode. As shown in Fig. 5(b), the photocurrent densities increase by 35.1 % and decrease by 8.5% for solid and liquid electrolytes under durative irradiation over 2 h,<sup>48</sup> respectively. Although two-hour test is far away for a stable DSSC, this preliminary result demonstrates that the stability of cell device can be significantly enhanced by utilizing  $\Gamma/I_3^-$  incorporated PEO/PANi solid electrolyte.<sup>49</sup>

#### 4. Conclusions

In summary, full-solid-state electrolytes from  $\Gamma/I_3^-$  incorporated PEO/PANi featured by catalytic activity and shortened charge diffusion path length have been fabricated by a facile blending process free of any additives and employed in assembling efficient DSSCs. It is demonstrated that  $\Gamma/I_3^-$  incorporated PEO/1.0 wt%PANi electrolyte has an optimal charge-transfer ability and electrocatalytic activity toward  $I_3^-$  reduction. Due to expanded reaction area for electrolyte/Pt interface to solid-state electrolyte system and shortened charge transfer path length, the kinetics for  $I_3^- \leftrightarrow \Gamma$  interconversion and dye recovery and therefore electron density on conduction band of  $TiO_2$  have been markedly enhanced. The DSSC employing  $\Gamma/I_3^-$  incorporated PEO/1.0 wt%PANi electrolyte exhibits an impressive power conversion efficiency of 6.1% in comparison with 0.8% from  $\Gamma/I_3^-$  incorporated PEO and 0.1% from pristine PANi-hole-transporting based devices. The research presented here is far from being optimized but these profound advantages along with

cost-effectiveness, mild synthesis, and scalable materials promise the  $\Gamma^-/I_3^-$  incorporated PEO/1.0 wt% PANi electrolytes to be strong candidates in full-solid-state DSSCs. Further studies are now in progress to extend this approach to other solid-state electrolytes for better photovoltaic performances.

## Acknowledgements

The authors gratefully acknowledge Fundamental Research Funds for the Central Universities (201313001, 201312005), Shandong Province Outstanding Youth Scientist Foundation Plan (BS2013CL015), Shandong Provincial Natural Science Foundation (ZR2011BQ017), Research Project for the Application Foundation in Qingdao (13-1-4-198-jch), National Natural Science Foundation of China (51102219, 51342008, U1037604), National High Technology Research and Development Program of China (2010AA09Z203, 2010AA065104), and National Key Technology Support Program (2012BAB15B02).

## References

- 1 S. S. Li and C. W. Chen, *J. Mater. Chem. A*, 2013, **1**, 10574–10591.
- 2 Q. Zhang, E. Uchaker, S. L. Candelaria and G. Z. Cao, *Chem. Soc. Rev.*, 2013, **42**, 3127–3171.
- 3 Q. H. Li, Y. Yuan, Z. Chen, X. Jin, T. H. Wei, Y. Li, Y. C. Qin and W. F. Sun, *ACS Appl. Mater. Interfaces*, 2014, **6**, 12798–12807.
- 4 O. Adebajo, B. Vaagensmith and Q. Q. Qiao, *J. Mater. Chem. A*, 2014, **2**, 10331–10349.
- 5 B. O'Regan and M. Grätzel, *Nature*, 1991, **353**, 737–740.
- 6 U. Bach and T. Daeneke, *Angew. Chem. Int. Ed.*, 2012, **51**, 10451–10452.

- 7 D. Kim, A. Ghicov, S. P. Albu and P. Schmuki, *J. Am. Chem. Soc.*, 2008, **130**, 16454–16455.
- 8 X. X. Chen, Q. W. Tang, B. L. He, L. Lin and L. M. Yu, *Angew. Chem. Int. Ed.*, 2014, **53**, 10799–10803.
- 9 E. J. W. Crossland, N. Noel, V. Sivaram, T. Leijtens, J. A. Alexander–Webber and H. J. Snaith, *Nature*, 2013, **495**, 215–219.
- 10 H. Choi, W. T. Chen and P. V. Kamat, *ACS Nano*, 2012, **6**, 4418–4427.
- 11 Q. W. Tang, H. Y. Cai, S. S. Yuan and X. Wang, *J. Mater. Chem. A*, 2013, **1**, 317–323.
- 12 M. Cheng, X. C. Yang, F. G. Zhang, J. H. Zhao and L. C. Sun, *Angew. Chem. Int. Ed.*, 2012, **51**, 9896–9899.
- 13 S. Mathew, A. Yella, P. Gao, R. Humphry–Baker, B. F. E. Curchod, N. Ashari–Astani, I. Tavernelli, U. Rothlisberger, M. K. Nazzeruddin and M. Grätzel, *Nat. Chem.*, 2014, **6**, 242–247.
- 14 J. H. Wu, Z. Lan, J. M. Lin, M. L. Huang, S. C. Hao, T. Sato and S. Yin, *Adv. Mater.*, 2007, **19**, 4006–4011.
- 15 Q. Dai, D. R. MacFarlane, P. C. Howlett and M. Forsyth, *Angew. Chem. Int. Ed.*, 2005, **44**, 313–316.
- 16 H. H. Snaith and L. Schmidt–Mende, *Adv. Mater.*, 2007, **19**, 3187–3200.
- 17 H. Wang, X. Zhang, F. Gong, G. Zhou and Z. S. Wang, *Adv. Mater.*, 2012, **24**, 121–124.
- 18 S. S. Yuan, Q. W. Tang, B. B. Hu, C. Q. Ma, J. L. Duan and B. L. He, *J. Mater. Chem. A*, 2014, **2**, 2814–2821.
- 19 S. S. Yuan, Q. W. Tang, B. L. He and P. Z. Yang, *J. Power Sources*, 2014, **254**, 98–105.
- 20 S. S. Yuan, Q. W. Tang, B. L. He and Y. Zhao, *J. Power Sources*, 2014, **260**, 225–232.

- 21 N. Cai, S. J. Moon, L. Cevey-Ha, T. Moehl, R. Humphry-Baker, P. Wang, S. M. Zakeeruddin and M. Grätzel, *Nano Lett.*, 2011, **11**, 1452–1456.
- 22 W. Zhang, Y. M. Cheng and X. Yin, B. Liu, *Macromol. Chem. Phys.*, 2011, **212**, 15–23.
- 23 H. J. Snaith and L. Schmidt-Mende, *Adv. Mater.*, 2007, **19**, 3187–3200.
- 24 I. K. Ding, J. Melas-Kyriazi, N. L. Cevey-Ha, K. G. Chittibabu, S. M. Zakeeruddin, M. Grätzel and M. D. McGehee, *Org. Electron.*, 2010, **11**, 1217–1222.
- 25 S. Günes, H. Neugebauer and N. S. Sariciftci, *Chem. Rev.*, 2007, **107**, 1324–1338.
- 26 Y. C. Hsu, L. C. Tseng and R. H. Lee, *J. Polym. Sci. Pol. Phys.*, 2014, **52**, 321–332.
- 27 S. S. Yuan, Q. W. Tang, B. L. He, L. Men and H. Y. Chen, *Electrochim. Acta*, 2014, **125**, 646–651.
- 28 J. H. Wu, Y. Li, Q. W. Tang, G. T. Yue, J. M. Lin, M. L. Huang and L. J. Meng, *Sci. Rep.*, 2014, **4**, 4028.
- 29 Q. Tai, B. Chen, F. Guo, S. Xu, H. Hu, B. Sebo and X. Z. Zhao, *ACS Nano*, 2011, **5**, 3795–3799.
- 30 Q. H. Li, J. H. Wu, Q. W. Tang, Z. Lan, P. J. Li, J. M. Lin and L. Q. Fan, *Electrochem. Commun.*, 2008, **10**, 1299–1302.
- 31 J. Yoon, M. Jin and M. Lee, *Adv. Mater.*, 2011, **23**, 3974–3978.
- 32 Q. W. Tang, J. H. Wu, X. M. Sun, Q. H. Li and J. M. Lin, *Langmuir*, 2009, **25**, 5253–5257.
- 33 Q. W. Tang, L. Lin, X. Zhao, K. Huang and J. H. Wu, *Langmuir*, 2012, **28**, 3972–3978.
- 34 X. Jiang, K. M. Karlsson, E. Gabrielsson, E. M. J. Johansson, M. Quintana, M. Karlsson, L. C. Sun, G. Boschloo and A. Hagfeldt, *Adv. Funct. Mater.*, 2011, **21**, 2944–2952.
- 35 Y. S. Kwon, J. Lim, I. Song, I. Y. Song, W. S. Shin, S. J. Moon and T. Park, *J. Mater. Chem.*, 2012, **22**, 8641–8648.

- 36 M. Wu, X. Lin, Y. Wang, L. Wang, W. Guo, D. Qi, X. Peng, A. Hagfeldt and M. Grätzel, *J. Am. Chem. Soc.*, 2012, **134**, 3419–3428.
- 37 M. K. Wang, A. M. Anghel, B. Marsan, N. C. Ha, N. Pootrakulchote, S. M. Zakeeruddin and M. Grätzel, *J. Am. Chem. Soc.*, 2009, **131**, 15976–15977.
- 38 Q. W. Tang, S. S. Yuan and H. Y. Cai, *J. Mater. Chem. A*, 2013, **1**, 630–636.
- 39 J. H. Yum, B. E. Hardin, S. J. Moon, E. Baranoff, F. Nüesch, M. D. McGehee, M. Grätzel and M. K. Nazeeruddin, *Angew. Chem. Int. Ed.*, 2009, **48**, 9277–9280.
- 40 D. Xu, C. Z. Shi, L. Wang, L. H. Qiu and F. Yan, *J. Mater. Chem. A*, 2014, **2**, 9803–9811.
- 41 P. J. Li, Y. Y. Duan, Q. W. Tang, B. L. He and R. Li, *J. Power Sources*, 2015, **273**, 180–184.
- 42 E. Lancelle–Beltran, P. Prene, C. Boscher, P. Belleville, P. Buvat and C. Sanchez, *Adv. Mater.*, 2006, **18**, 2579–2582.
- 43 G. K. Mor, S. Kim, M. Paulose, O. K. Varghese, K. Shankar, J. Basham and C. A. Grimes, *Nano Lett.*, 2009, **9**, 4250–4257.
- 44 S. R. Jang, K. Zhu, M. J. Ko, K. Kim, C. Kim, N. G. Park and A. J. Frank, *ACS Nano*, 2011, **5**, 8267–8274.
- 45 V. Armel, J. M. Pringle, P. Wagner, M. Forsyth, D. Officer and D. R. MacFarlane, *Chem. Commun.*, 2011, **47**, 9327–9329.
- 46 U. Bach, D. Lupo, P. Comte, J. E. Moser, F. Weissortel, J. Salbeck, H. Spreitzer and M. Grätzel, *Nature*, 1998, **395**, 583–585.
- 47 Z. Y. Tang, J. H. Wu, M. Zheng, J. H. Huo and Z. Lan, *Nano Energy*, 2013, **2**, 622–627.
- 48 B. L. He, X. Meng and Q. W. Tang, *ACS Appl. Mater. Interfaces*, 2014, **6**, 4812–4818.
- 49 L. Xi, X. C. Yang, J. J. Gao, H. N. Tian, J. Z. Zhao, A. Hagfeldt and L. C. Sun, *J. Am. Chem. Soc.*, 2011, **133**, 8458–8460.

